Nanoscale Research Letters

NANO IDEA Open Access

Coupled Resonance Enhanced Modulation for a Graphene-Loaded Metamaterial Absorber

Dong Xiao, Qiang Liu, Lei Lei, Yiling Sun, Zhengbiao Ouyang and Keyu Tao*

Abstract

A graphene-loaded metamaterial absorber is investigated in the mid-infrared region. The light-graphene interaction is greatly enhanced by virtue of the coupled resonance through a cross-shaped slot. The absorption peaks show a significant blueshift with increasing Fermi level, enabling a wide range of tunability for the absorber. A simple circuit model well explains and predicts this modulation behavior. Our proposal may find applications in a variety of areas such as switching, sensing, modulating, and biochemical detecting.

Keywords: Metamaterials, Graphene, Broadband modulation, Coupled-resonance, Mid-infrared absorber

Background

Plasmonic metamaterial (PM) absorbers work with metallic nanostructures at deep subwavelength scale. Perfect absorptions can be achieved and tailored at particular wavelengths, leading to a variety of applications including light emitter/detector, sensor, photothermal therapy, optical-mechanical interaction, and hyperspectral imaging [1–7]. PM absorbers also provide a promising platform for designing novel functional devices with tunable properties. By introducing components such as liquid crystals, semiconductors, or phase-change materials, the optical response can be modulated electrically, optically, or thermally [8–13], which enables new types of modulators, switches, and multispectral detectors.

Most recently, graphene has received considerable attention because of its high-speed modulation capability and tunability as a plasmonic material [14–20]. Specifically, the graphene conductivity depends on the Fermi level (E_F) which can be continuously tuned through bias voltage within several nanoseconds, enabling a high modulation rate in the near infrared and mid-infrared regions [17, 19–24]. However, as the single graphene layer is only atomically thick, the interaction between the incident light and the plasmonic resonance is quite weak. And this interaction becomes even weaker in the mid-infrared area due to the Pauli blocking of interband transitions [22]. As a result, the wavelength tuning range as well as the modulation depth is quite limited. The wavelength shift is generally less than 10% of the resonance wavelength [21, 22, 25–28], which is still a challenge for practical applications in optical communications and wideband spectral detections. Thus, in order to achieve efficient electro-optical modulation, the graphene-light interaction needs to be greatly strengthened. Some progresses have been made in previous studies. Based on the designs of complex nanostructures such as nano-antennas and split ring resonators [19, 21, 22, 25, 27, 28], the enhancement of graphene-light interaction has been theoretically and experimentally demonstrated. Yet, these designs are usually complicated or polarization-dependent, the range of working frequency is relatively small and the tunability is still limited.

In this work, we have proposed a graphene-loaded absorber with modulation range from 9 to 14 μm, which is of great interest for applications such as biochemical sensing and thermal imaging [5, 29–31]. The coupled-resonances inside the cross-shaped slot offer four orders of enhancement for the electric field, strongly intensifying the graphene-light interaction and resulting in a shift of up to 25% in the central wavelength. In addition, we propose a simple LC circuit model which well explains

* Correspondence: taokeyu@szu.edu.cn
THz Technical Research Center of Shenzhen University, Shenzhen Key Laboratory of Micro-Nano Photonic Information Technology, Key Laboratory of Optoelectronic Devices and Systems of Ministry of Education and Guangdong Province, College of Electronic Science and Technology, Shenzhen University, Shenzhen 518060, China

and predicts the graphene-induced modulation controlled by the voltage and geometric parameters. Such a large range of tunability would be promising in many applications.

Methods

As shown in Fig. 1a, patterned metallic patches are arranged with a period of $\Lambda = 8\,\mu m$ on the metal substrate separated by a dielectric spacer. A single layer of graphene sandwiches between the patches and the spacer. The substrate is very thick and acts as a reflection mirror. The thickness of the spacer layer is $t_d = 520\,nm$ and that of the metallic patches is $t_m = 100\,nm$. Figure 1b shows the top view of one unit cell. Two subunits are arranged in a diagonal symmetry in order to support the polarization independence. A cross-shaped slot is etched on each square patch, dividing it into four small identicals. The sizes of the small identicals in S_1 and S_2 are $l_1 = 1.5\,\mu m$ and $l_2 = 1.7\,\mu m$, respectively. The slot width for both subunits is $a = 20\,nm$. In our study, the metallic material is chosen as gold (Au), whose optical property is described by the Drude model of $\varepsilon(\omega) = 1 - \omega_p^2/(\omega(\omega + \tau))$ with $\omega_p = 1.369 \times 10^{16}\,Hz$ and $\tau = 1.224 \times 10^{14}\,Hz$ [32]. The dielectric spacer is composed of zinc sulfide (ZnS), whose optical index is $n = 2.2$ with negligible loss in the mid-infrared region [33].

The finite-difference time-domain (FDTD; Lumerical FDTD Solutions) method is employed to calculate reflectance spectra and electromagnetic field distribution. The simulations are carried out with periodic boundary conditions in the x and y directions and perfect matched layer conditions in the z directions. The single graphene layer is modeled as a two-dimensional structure by the surface conductivity approach [34]. The surface conductivity of the graphene layer σ_g, including the interband term σ_{inter} and the intraband term σ_{intra}, can be calculated by the Kubo formula [35].

$$\begin{aligned}\sigma_g(\omega, E_F, \Gamma, T) &= \sigma_{intra} + \sigma_{inter} \\ &= \frac{-ie^2}{\pi\hbar^2(\omega + i2\Gamma)} \int_0^\infty \xi \left(\frac{\partial f_d(\xi)}{\partial \xi} - \frac{\partial f_d(-\xi)}{\partial \xi} \right) d\xi \\ &\quad + \frac{ie^2(\omega + i2\Gamma)}{\pi\hbar^2} \int_0^\infty \xi \left(\frac{f_d(-\xi) - f_d(\xi)}{(\omega + i2\Gamma)^2 - 4(\xi/\hbar)^2} \right) d\xi \end{aligned} \quad (1)$$

where e and ξ are the charge and energy of the electron, $\hbar$ is the reduced plank's constant, ω is the angular frequency, $f_d \equiv 1/(e^{(\xi - E_F)/k_B T} + 1)$ refers to the Fermi-Dirac distribution, T is the absolute temperature, Γ is the scattering rate, k_B is the Boltzmann constant, and E_F is the Fermi level. In our calculation, $T = 300\,K$, and $\Gamma = 10$ meV [28]. The mesh size near the graphene layer is 0.25 nm, and 2.5 nm in the slots. The effective permittivity of graphene can then be expressed as

$$\varepsilon_g = 1 + i\sigma_g / (\varepsilon_0 \omega t_g) \quad (2)$$

where ε_0 is the permittivity of vacuum, and t_g is the thickness of graphene layer. Equations (1) and (2) demonstrate that the optical constants of graphene change with E_F. This change leads to tunability of the absorption frequency, whose range can be greatly enlarged by the coupled resonance in the nanostructures, substantially lowering the applied voltage in devices.

Results and Discussion

Figure 2a shows the absorption spectra for x-polarized wave ($\phi = 0$) at the normal incidence. When the Fermi level is $E_F = 0eV$, two absorption peaks are observed at the wavelength $\lambda = 12.4\,\mu m$ and $13.3\,\mu m$, respectively. The incident light ranging from 12.1 to $13.5\,\mu m$ is almost absorbed by the nanostructure. As E_F increases, the resonance moves toward shorter wavelength. At $E_F = 0.2\,eV$, the absorption peaks shift

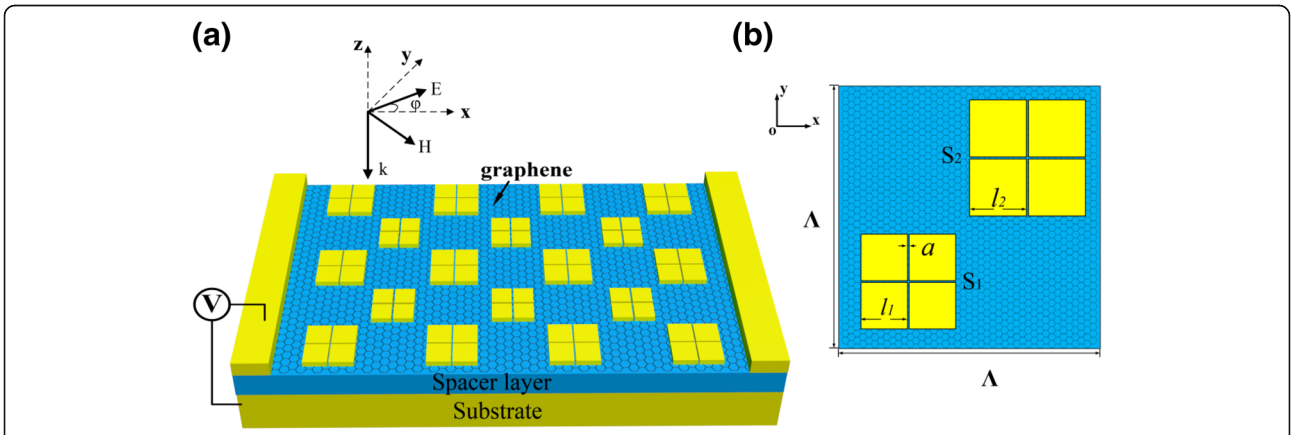

Fig. 1 **a** Schematic diagram of the proposed graphene-loaded metamaterial. The cross-shaped slot in each subunit enables a great enhancement of graphene-light interaction without polarization dependence. **b** Top view of the structure in one period. Two subunits are arranged diagonally with different patch sizes

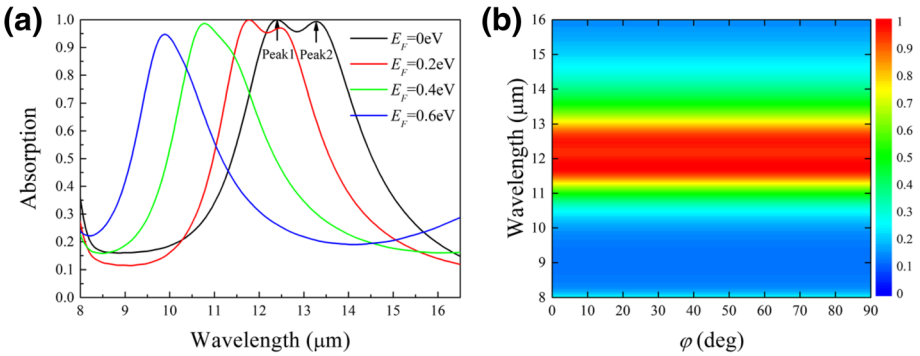

Fig. 2 Absorption spectra at the normal incidence with different E_F at $\varphi = 0$, showing large blueshift of the peaks with increasing E_F (**a**), and with different φ at $E_F = 0.2$eV, demonstrating a polarization independence (**b**). The polarization angle φ is defined as in Fig. 1a

to 11.8 μm and 12.46 μm, indicating respectively a relative shift of 4.8% and 6%. Meanwhile, the absorbance of peak 2 declines, which is attributed to the impedance mismatch between the metamaterial and air at a higher E_F [28]. Here, it is interesting that peak 2 blueshifts faster than peak 1 as the Fermi level keeps increasing. This observed behavior will be explained later by a circuit model.

The modulation can be quantified by a parameter $M = \Delta\lambda/\lambda_0$, where λ_0 is the resonance wavelength at $E_F = 0$ eV and $\Delta\lambda$ is the wavelength shift due to the change of E_F. Figure 2a shows $M_1 = 20.1\%$ and $M_2 = 25.5\%$ for peak 1 and peak 2, respectively, when E_F reaches 0.6 eV. The modulation range of resonances is much broader compared with previous works [19, 21, 22, 25–28]. Such a large modulation at a low E_F is highly desirable for many applications. Separate calculations show that the absorption peaks blueshift with decreasing thickness of the spacer (Additional file 1). Thus, we can optimize the thickness to set a suitable start point of modulation. In addition, the optical response of the proposed metamaterial is polarization-independent as shown in Fig. 2b. The absorption spectrum keeps unchanged when the polarization angle ϕ varies from 0 to 90°, owing to the symmetry of the design.

The mechanism of perfect absorptions is clearly illustrated by the field distributions at the resonances. Because of the well-known metal-insulator-metal (MIM) structure [3, 32, 36–38] shown in Fig. 1, localized SPPs are stimulated to form compact magnetic resonances in each patch. Figure 3a and b demonstrate the normalized magnetic field $|H|^2$ in the graphene layer for $E_F = 0.2$ eV at the resonance wavelengths of $\lambda_1 = 11.8$ μm and $\lambda_2 = 12.46$ μm, respectively. Since the SPPs are strongly localized, two subunits can work independently. However, due to the narrow width of the splitting slot inside each subunit, the resonances of the four identicals are actually coupled to each other. And this coupling tremendously increases the electric field inside the slot, as shown in Fig. 3c and d. Only the E fields in the y-direction slot are obvious here because the incident light is in the x polarization. The intensity of the E field enhanced by the resonance coupling is four orders of magnitude larger than that of the incident light E_{inc}. In contrast, the most intensified fields used for modulation in previous work are at the patch edges. Figure 3e and f show the sharp comparison of the enhancements between the slots and edges along the white line in Fig. 3c and d, respectively.

Such field distributions well explain the reason why the modulation is so great in our proposal. Based on a perturbation theory, the graphene-induced shifting of resonance can be evaluated as $\Delta\omega = -i\sigma_g \int_S |E_s|^2 dS / W_0$ [22]. Here, $|E_s|^2$is the intensity of the electric field in the graphene layer, W_0 is the stored energy, and S denotes the area covered by the graphene. The spectral shift of the resonance ($\mathrm{Re}(\Delta\omega)$) is decided by the imaginary part of σ_g, which is much greater than its real part in the mid-infrared region [22, 28]. As clearly shown in the Fig. 3c–f, the enhancement of electric field inside the narrow slot is more than 10 times of that at the edges. As a result, the integral value is mainly contributed by the greatly enhanced E field in the patch slots, leading to a much bigger shift of the peaks than in previous cases which only possess the enhanced E fields at the metallic edges [21, 22, 25, 27, 28].

According to the field distributions and above discussions, an LC circuit model is proposed to study the tuning behavior. As shown in Fig. 4a, L_i and C_i ($i = 1, 2$) are, respectively, the inductance and capacitance for the patch S_i in Fig. 1b. When the slot width a is very big and there is no graphene layer, we can ignore the effects induced by the slots and graphene. Then, L_i and C_i can be decided by separate calculations through fitting with the resonant wavelength obtained in absorption spectra [37, 39, 40]. The results are $L_1 = 0.07$ pH and $C_1 = 350$ aF for

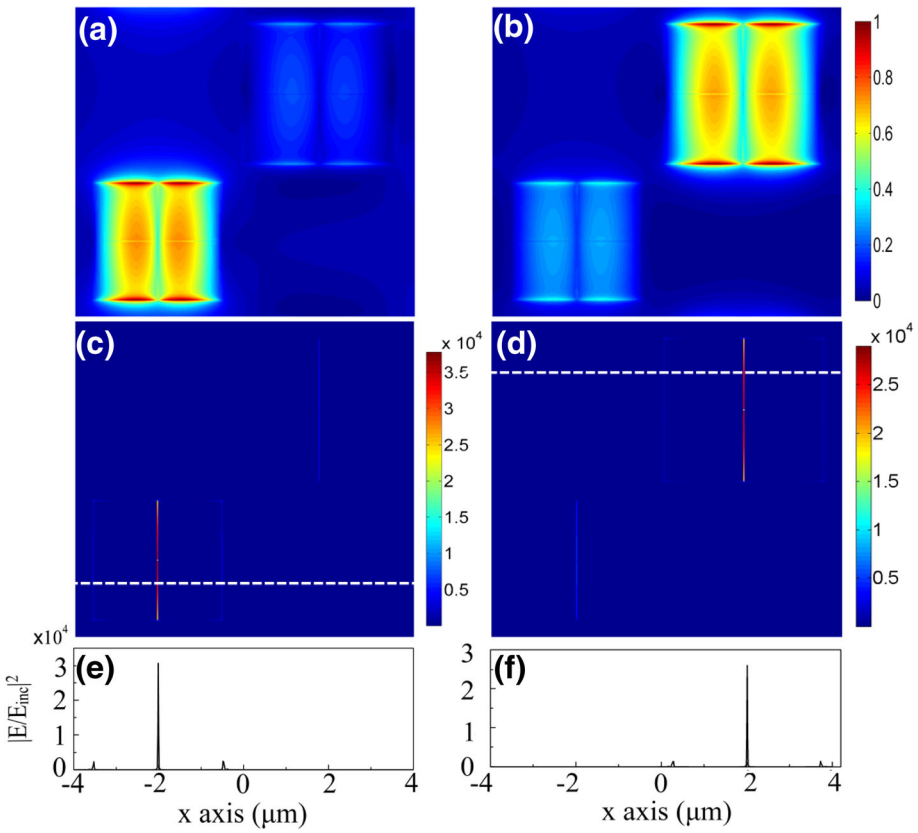

Fig. 3 Field distributions in the graphene layer at $E_F = 0.2$ eV for the x-polarized light at the normal incidence, showing great enhancement in the slot caused by the coupled-resonances. **a, b** Normalized magnetic field $|H|^2$ at $\lambda_1 = 11.8$ μm (**a**) and $\lambda_2 = 12.46$ μm (**b**); **c**, **d** The corresponding field distribution of $|E/E_{inc}|^2$; **e**, **f** $|E/E_{inc}|^2$ along the white dash-line shown in **c** and **d**, respectively. A sharp contrast is seen between the intensity inside the slot and that at the patch edges, giving hints for much wider tuning range than that in previous works

subunit S_1, while $L_2 = 0.075$ pH and $C_2 = 380$ aF for subunit S_2. The slot-induced coupling effect inside each subunit can be described by a shunt capacitance C_c, which is found to decrease with the increasing slot width a. In our cases, C_c is 290 aF for $a = 20$ nm, and becomes 200 aF, 180 aF, and 135 aF with every increasing 10 nm of a. The resonance wavelength is obtained by letting the impedance of the circuit to be zero, i.e., $\lambda_i^0 = 2\pi c_0\sqrt{L_i C_i^0}$. Here, c_0 is the light speed in vacuum, "i" refers to subunit S_i, and $C_i^0 = C_i + C_c$.

The two-dimensional graphene layer basically acts as an inductor. As shown in Fig. 3, the main contribution of the graphene layer comes from the slot position where the electric field is intensified. Since the slot width is much smaller than the operating wavelength and the wavelength of graphene plasmon, the quasi-static approximation is valid. The voltage V and the current I across the slot can be evaluated by $V = aE$ and $I = 2l_i t_g(\sigma_g - i\omega\varepsilon_0)E$, where E is the electric field in the graphene layer. So, we can introduce an inductance $L_g = -1/\omega\,\mathrm{Im}(V/I)$ [41], which describes the contribution of the graphene layer and is found to be

$$L_g = \frac{a}{2l_i\omega^2\varepsilon_0|\,\mathrm{Re}(\varepsilon_g)|t_g} \quad (i = 1, 2) \tag{3}$$

This inductor serves as a parallel element shown in Fig. 4a. As a result, the total inductance of one patch is obtained by $1/L_i' = 1/L_i + 1/L_g$. The final resonance wavelength of each subunit, with the graphene layer, becomes

$$\lambda_i' = 2\pi c_0\sqrt{L_i' C_i^0} \quad (i = 1, 2) \tag{4}$$

Because each subunit works independently, the total impedance of the metamaterial can be obtained from the parallel connection of the impedances of the two subunits.

This LC model predicts a blueshift of the resonance with increasing E_F. Deduced from Eqs. (1) and (2), we get a larger value of $|\mathrm{Re}(\varepsilon_g)|$ for the graphene at a higher E_F, which gives a smaller L_g in Eq. (3). Because of the parallel connection of the inductors, the final inductor

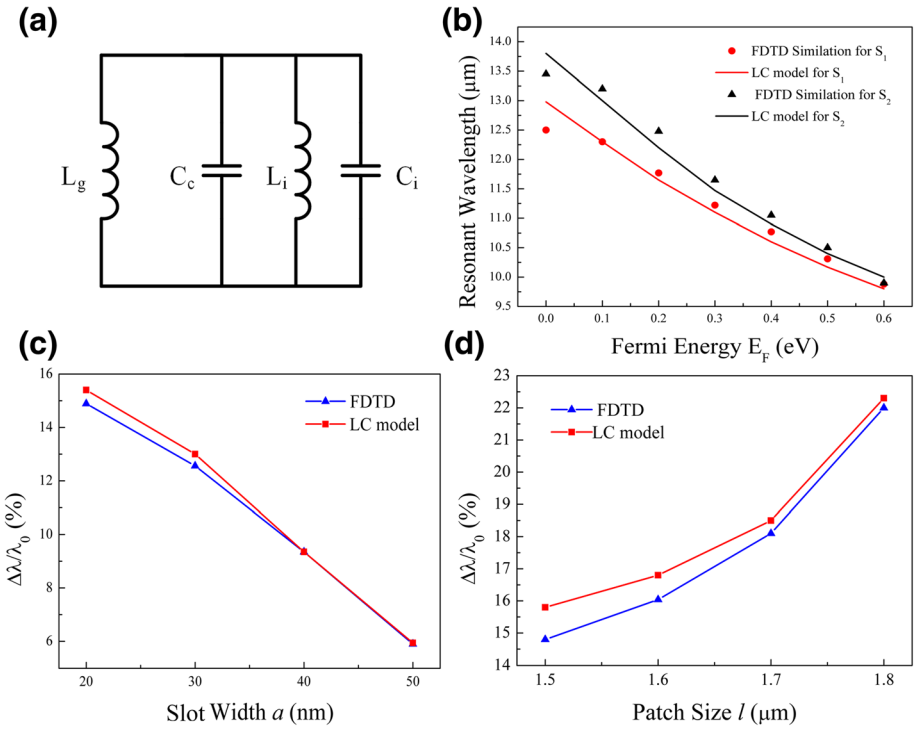

Fig. 4 **a** An LC circuit model includes contributions from separate patches ($L_i$and C_i), slot (C_c), and graphene (L_g). **b** Resonances calculated by the LC model compared with FDTD simulations. **c**, **d** Resonance shift for a single patch at $E_F = 0.4$ eV with changing geometrical parameter of **c** slot width ($l = 1.5$ μm) and **d** patch size ($a = 20$ nm)

L_i' becomes smaller, leading to a shorter wavelength of resonance in Eq. (4). The calculated result is summarized in Fig. 4b, showing a good agreement with the resonant wavelength obtained by the FDTD simulations. Small deviation is seen because our LC model ignores the contribution of weak fields at the edges of each patch (Fig. 3c–f). The LC model also shows how the geometric parameters influence the blueshift of the resonance. Differentiating Eq. (4), we have $\partial\lambda_i'/\partial L_i' \propto 1/\sqrt{L_i'}$. It is obvious that a small value of $\sqrt{L_i'}$ is favored to increase the sensitivity of this blueshift. Because the inductors are parallelly connected and L_i is fixed, a small value of the total inductance L_i' means a small value of the graphene inductance L_g. In order to increase the tuning range, the slot width a should be small and the patch size l be large, according to Eq. (3). Figure 4c shows that the blueshift of resonance at $E_F = 0.4$ eV increases from around 6 to 15%, when the slot width inside S_1 decreases from 50 to 20 nm. On the other hand, if we fix the slot width at $a = 20$ nm, the resonance increases from 15 to 22% with patch size changing from 1.5 to 1.8 μm as shown in Fig. 4d. The good agreement with the FDTD simulations demonstrates that such a simple circuit model is an efficient method for studying related metamaterials devices.

Conclusions

In conclusion, we have designed a polarization-independent, broadband metamaterial absorber with a large range of modulation. For both resonances, the tuning range reach up to 20.1% and 25.5% of the central wavelength when E_F increases from 0 to 0.6 eV. Such a large modulation comes from the graphene-light interaction tremendously enhanced by the coupled-resonances inside the cross-shaped slot of each metallic patch. This effect is well described by a graphene-introduced inductor in the LC model. Such a simple model predicts the modulation behavior under different geometric parameters, and the results agree well with the FDTD simulations. Our proposal is beneficial to potential applications such as optical communication, sensing, and thermal imaging.

Additional file

Additional file 1: Supplementary Material. (PDF 308 kb).

Abbreviations

E_F: Fermi level; FDTD: Finite-different time-domain; MIM: Metal-insulator-metal; PM: Plasmonic metamaterial; ZnS: Zinc sulfide

Acknowledgements

Not applicable.

Funding
This work was supported by the Chinese Natural Science Foundation (Grant Nos. 61107049, 11734012), Basic Research Program of Shenzhen (JCYJ20170302151033006), Natural Science Foundation of Guangdong Province (2017A030310131).

Availability of Data and Materials
All date can be provided on a suitable request.

Authors' Contributions
DX conducted the simulations and processed the data and figures. All authors participated in discussions. KYT, DX, ZBOY, QL, and LL prepared the manuscript. KYT supervised the whole work. All authors read and approved the final manuscript.

Competing Interests
The authors declare that they have no competing interests.

Publisher's Note

Received: 4 October 2018 Accepted: 2 January 2019
Published online: 22 January 2019

References

1. Zhu H, Yi F, Cubukcu E (2016) Plasmonic metamaterial absorber for broadband manipulation of mechanical resonances. Nat Photonics 10(11):709
2. Ndukaife JC, Shalaev VM, Boltasseva A (2016) Plasmonics—turning loss into gain. Science 351:334–335
3. Xie Q, Dong G, Wang B-X, Huang W-Q (2018) Design of quad-band terahertz metamaterial absorber using a perforated rectangular resonator for sensing applications. Nanoscale Res Lett 13:137
4. Wang H, Chen Q, Wen L, Song S, Hu X et al (2015) Titanium-nitride-based integrated plasmonic absorber/emitter for solar thermophotovoltaic application. Photonics Research 3:329–334
5. Tittl A, Michel AKU, Schäferling M, Yin X, Gholipour B et al (2015) A switchable mid-infrared plasmonic perfect absorber with multispectral thermal imaging capability. Adv Mater 27:4597–4603
6. Li H, Qin M, Wang L, Zhai X, Ren R et al (2017) Total absorption of light in monolayer transition-metal dichalcogenides by critical coupling. Opt Express 25:31612–31621
7. Li H, Ren Y, Hu J, Qin M, Wang L (2018) Wavelength-selective Wide-angle Light Absorption Enhancement in Monolayers of Transition-Metal Dichalcogenides. J Lightwave Technol. 36(16):3236–3241
8. Yang A, Yang K, Yu H, Tan X, Li J et al (2016) Piezoelectric tuning of narrowband perfect plasmonic absorbers via an optomechanic cavity. Opt Lett 41:2803–2806
9. Carrillo SG-C, Nash GR, Hayat H, Cryan MJ, Klemm M et al (2016) Design of practicable phase-change metadevices for near-infrared absorber and modulator applications. Opt Express 24:13563–13573
10. Zhu Z, Evans PG, Haglund RF Jr, Valentine JG (2017) Dynamically reconfigurable metadevice employing nanostructured phase-change materials. Nano Lett 17:4881–4885
11. Song Z, Wang Z, Wei M (2019) Broadband tunable absorber for terahertz waves based on isotropic silicon metasurfaces. Mater Lett 234:138–141
12. Song Z, Wang K, Li J, Liu QH (2018) Broadband tunable terahertz absorber based on vanadium dioxide metamaterials. Opt Express 26:7148–7154
13. Chu Q, Song Z, Liu QH (2018) Omnidirectional tunable terahertz analog of electromagnetically induced transparency realized by isotropic vanadium dioxide metasurfaces. Appl Phys Express 11:082203
14. Guo Z, Nie X, Shen F, Zhou H, Zhou Q et al (2018) Actively tunable terahertz switches based on subwavelength graphene waveguide. Nanomaterials 8:665
15. Luo L, Wang K, Ge C, Guo K, Shen F et al (2017) Actively controllable terahertz switches with graphene-based nongroove gratings. Photonics Research 5:604–611
16. Emani NK, Chung T-F, Kildishev AV, Shalaev VM, Chen YP et al (2013) Electrical modulation of Fano resonance in plasmonic nanostructures using graphene. Nano Lett 14:78–82
17. He X, Zhao Z-Y, Shi W (2015) Graphene-supported tunable near-IR metamaterials. Opt Lett 40:178–181
18. Yu R, Pruneri V, García de Abajo FJ (2015) Resonant visible light modulation with graphene. ACS Photonics 2:550–558
19. Zeng B, Huang Z, Singh A, Yao Y, Azad AK et al (2018) Hybrid graphene metasurfaces for high-speed mid-infrared light modulation and single-pixel imaging. Light Sci Appl 7:51
20. Li H, Wang L, Liu J, Huang Z, Sun B et al (2013) Investigation of the graphene based planar plasmonic filters. Appl Phys Lett 103:211104
21. Yao Y, Kats MA, Shankar R, Song Y, Kong J et al (2014) Wide wavelength tuning of optical antennas on graphene with nanosecond response time. Nano Lett 14:214–219
22. Dabidian N, Kholmanov I, Khanikaev AB, Tatar K, Trendafilov S et al (2015) Electrical switching of infrared light using graphene integration with plasmonic Fano resonant metasurfaces. ACS Photonics 2:216–227
23. Chen Y, Yao J, Song Z, Ye L, Cai G et al (2016) Independent tuning of double plasmonic waves in a free-standing graphene-spacer-grating-spacer-graphene hybrid slab. Opt Express 24:16961–16972
24. Li H, Ji C, Ren Y, Hu J, Qin M et al (2019) Investigation of multiband plasmonic metamaterial perfect absorbers based on graphene ribbons by the phase-coupled method. Carbon 141:481–487
25. Mousavi SH, Kholmanov I, Alici KB, Purtseladze D, Arju N et al (2013) Inductive tuning of Fano-resonant metasurfaces using plasmonic response of graphene in the mid-infrared. Nano Lett 13:1111–1117
26. Liao Y-L, Zhao Y (2017) Graphene-based tunable ultra-narrowband mid-infrared TE-polarization absorber. Opt Express 25:32080–32089
27. Zhang YP, Li TT, Chen Q, Zhang HY, O'Hara JF et al (2015) Independently tunable dual-band perfect absorber based on graphene at mid-infrared frequencies. Sci Rep 5:18463
28. Vasić B, Gajić R (2013) Graphene induced spectral tuning of metamaterial absorbers at mid-infrared frequencies. Appl Phys Lett 103:261111
29. Rodrigo D, Limaj O, Janner D, Etezadi D, De Abajo FJG et al (2015) Mid-infrared plasmonic biosensing with graphene. Science 349:165–168
30. Vollmer M, Mollmann, KP (2010) Infrared Thermal Imaging|Fundamentals, Research and Applications. Wiley-VCH, Weinheim
31. Guo Q, Yu R, Li C, Yuan S, Deng B, et al. (2018) Efficient electrical detection of mid-infrared graphene plasmons at room temperature. Nat Mater 17: 986–992
32. Liu N, Mesch M, Weiss T, Hentschel M, Giessen H (2010) Infrared perfect absorber and its application As plasmonic sensor. Nano Lett 10:2342–2348
33. Palik ED (1985) Handbook of optical constants of solids. Academic Press, New York
34. Hanson GW (2008) Dyadic Green's functions and guided surface waves for a surface conductivity model of graphene. J Appl Phys 103:064302
35. Gusynin V, Sharapov S, Carbotte JP (2006) Magneto-optical conductivity in graphene. J Phys-Condens Mat 19(2):026222
36. Wu D, Li R, Liu Y, Yu Z, Yu L et al (2017) Ultra-narrow band perfect absorber and its application as plasmonic sensor in the visible region. Nanoscale Res Lett 12:427
37. Xiao D, Tao K, Wang Q (2016) Ultrabroadband mid-infrared light absorption based on a multi-cavity plasmonic metamaterial array. Plasmonics 11:389–394
38. Xiao D, Tao K (2015) Ultra-compact metamaterial absorber for multiband light absorption at mid-infrared frequencies. Appl Phys Express 8:102001
39. Matsuno Y, Sakurai A (2017) Perfect infrared absorber and emitter based on a large-area metasurface. Optical Materials Express 7:618–626
40. Tassin P, Koschny T, Kafesaki M, Soukoulis CM (2012) A comparison of graphene, superconductors and metals as conductors for metamaterials and plasmonics. Nat Photonics 6:259
41. Yao Y, Kats MA, Genevet P, Yu N, Song Y et al (2013) Broad electrical tuning of graphene-loaded plasmonic antennas. Nano Lett 13:1257–1264